RSC Advances

ROYAL SOCIETY OF CHEMISTRY

www.rsc.org/advances

Graphic Abstract

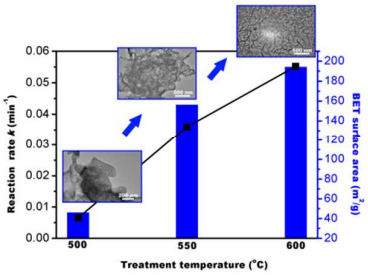

Nanostructured g-C_3N_4 with high surface area from heat treatment of guanidinium cyanurate exhibits better optical properties and enhanced photocatalytic activity.

Nanoporous photocatalysts developed through heat-driven stacking of graphitic carbon nitride nanosheets

Zhijun Huang, Fengbo Li*, Bingfeng Chen, and Guoqing Yuan*

Nanoporous graphitic carbon nitride was prepared through direct heat treatment of guanidinium cyanurate at 550-600 ℃ in air atmosphere. BET surface area of the resulting materials can reach 200 m^2/g. High porosity was developed through a heat-driven stacking of g-C_3N_4 nanosheets. The mechanism was detailedly revealed through TEM and N_2 adsorption measurement. Large-size g-C_3N_4 nanosheets are formed at 550℃ and stacked in a state similar to randomly creased paper slips. Further increase of treatment temperature to 600℃ results in curl and fragmentation of g-C_3N_4 nanosheets, which build up a highly porous matrix. Nanoporous graphitic carbon nitride with higher surface area exhibits better optical properties and have enhanced photocatalytic activity. The nanoporous g-C_3N_4 shows high photocatalytic activity for decomposition of rhodamine (RhB) in an aqueous solution.

1. Introduction

Photocatalysis has shown its importance in the energy and environmental applications since the discovery of water photolysis over TiO_2 electrode in 1972 [1]. There are many types of photocatalysts such as metal oxides, sulfides, nitrides and phosphides [2]. Many efforts have been put into the development of efficient, stable, low-cost and environmentally benign photocatalyst. Graphitic carbon nitride (g-C_3N_4) is a metal-free organic semiconductor and active for H_2 evolution from water under visible light irradiation in the presence of a sacrificial donor [3]. Graphitic-C_3N_4 has many special properties such as inexpensive precursors, facile preparation, non-toxicity, excellent stability and unique band structure [4].

Graphitic-C_3N_4 is synthesized by condensation of precursors containing carbon and nitrogen, such as cyanamide, dicyanamide or melamine [5]. Many strategies have been employed to enhance its catalytic performance, such as doping with heteroatoms [6], coupling with other semiconductors [7], coupling with carbon materials or polymers [8], surface modification [9], copolymerization [10] and texture modification[11].

Two-dimensional nanosheets are expexted to possess exceptional optical, electronic and mechanical properties and show application potential in sensors, electronics, catalysis, and energy conversion [12]. Graphitic-C_3N_4 is constituted by two-dimensional tri-*s*-triazine units connected with planar amino groups. Each layer is connected by weak van der Waals force, which is similar to graphite. Inspired by graphite and graphene, g-C_3N_4 nanosheets are synthesized to further develop its applications [13]. Graphitic-C_3N_4 nanosheets of around 2 nm were prepared through thermal oxidation etching of bulk g-C_3N_4 in air [13a]. Chemical exfoliation by H_2SO_4 is another effective method to synthesize g-C_3N_4 nanosheets [13b]. Under controlled conditions, single layer g-C_3N_4 nanosheets with large S_{BET} and enhanced photogenerated charge carrier transport were obtained. Ultrasonic assistant liquid exfoliation has been commonly employed for the fabrication of inorganic nanosheets from their parent layered materials [14]. Ultrathin g-C_3N_4 nanosheets have been successfully synthesized through this cost-effective route [13c-k]. In addition to photocatalyst, the two-dimensional nanosheets prepared by liquid exfoliation also show promising applications in bioimaging, electrochemiluminescence detection, disinfection, metal ions detection and drug nanocarriers because of the unique optical and electronic properties. However, liquid exfoliation is time consuming and not suitable for large-scale applications.

Recently, urea, an oxygen-containing precursor, was used for the synthesis of g-C_3N_4 [15]. Gas bubbles stemmed from oxygen result in g-C_3N_4 with platelet-like or porous morphology. Other precursors with heteroatom can also be used for the synthesis of g-C_3N_4 with or without the assistant of templates [16]. Owing to the peculiar nanostructures, large S_{BET} and enhanced optical and electronic properties, most of as-prepared g-C_3N_4 nanostructures exhibit enhanced catalytic activity.

In this work, guanidinium cyanurate (GC) was used as a novel precursor. Nanostructured g-C_3N_4 (CNG) was easily prepared through GC self-condensation under heat treatment during 450-600 ℃ in air atmosphere without the assistance of any template. The resultant materials had a stacking microstructure of g-C_3N_4 nanosheets. Self-condensation temeprature is the key parameter to determine the stacking model of g-C_3N_4. Three typical stacking models were observed with the incease of treatment temperature. The BET surface area of as-synthesized materials at 600 ℃ nearly reaches 200 m^2/g. Heat-driven stacking mechanism was detailedly revealed through TEM and N_2 adsorption measurement. The catalytic performance of g-C_3N_4 nanosheets was evaluated by rhodamine (RhB) degradation under light irritation, and compared with that of samples and prepared from melamine (CNM) and urea (CNU) under the same conditions.

2. Experimental

2.1. Preparation of catalysts

All the reagents were analytical-grade and used as received. Guanidinium cyanurate (GC) was synthesized according to the literature [17]. CNG were synthesized by directly heating of GC in air. Typically, 5 g of GC was placed in a covered crucible and then heated to a certain temperature in muffle furnace for 4 h with a heating rate of 10 ℃ min^{-1}. For comparison, CNM and CNU were also synthesized from melamine and urea respectively at 550℃ under the same heating conditions.

2.2. Characterization and methods

The powder X-ray diffraction (XRD) measurements were performed with Rigaku Rotaflex diffractometer equipped with Cu Kα radiation source (40 kV, 200 mA; λ= 1.54056 Å). Fourier transform infrared (FT-IR) spectra were recorded on a Bruker Tensor 27 by using KBr pellets. X-ray photoelectron spectroscopy (XPS) dates were obtained on a Thermo Scientific ESCALab 250Xi using 200 W monochromated Al Kα radiation. The Scanning electron microscopy (SEM) images were obtained on a Hitachi S-4800 instrument. The transmission electron microscopy (TEM) images were obtained on a JEOL JSM-2100 instrument with an accelerating voltage of 200 kV. The nitrogen adsorption-desorption experiments were performed at 77.3 K by a Quanta-chrome Autosorb Automated Gas Sorption System (Quantachrome Corporation). Before experiments, the samples were dried at 350 ℃ under vacuum for 6 h. The UV-visible absorption spectra were obtained using a UV-visible spectrometer (Shimadzu UV-2600) equipped with an integrating sphere assembly. $BaSO_4$ was used as reference. Photoluminescence spectra (PL) were recorded with a Hitachi F-4500 fluorescence spectrometer with excitation at 350 nm.

2.3 Photocatalytic actvity test

The photocatalytic activities of the prepared g-C_3N_4 were evaluated by the degradation of 10 mg/L RhB at room temperature under light irradiation. The light was provided by a 500 W xenon lamp. Typically, 150 mL of RhB aqueous solution and 20 mg g-C_3N_4 were mixed in a 250 mL quartz reactor. Prior to irradiation, the suspension was stirred in the dark for 1 h to ensure adsorption-desorption equilibrium. About 4 mL of suspension was sampled at 10 min interval. After centrifugation, the upper clear liquid was analyzed by UV-visible absorption spectra. The maximum absorption was recorded at 553 nm and used for evaluating the concentration of RhB.

The degradation rate and rate constant k are calculated by equation (1) and (2) respectively as follows:

$$\text{Degradation rate} = (C_0 - C)/C_0 \times 100\% \quad (1)$$

$$\ln(C/C_0) = -kt \quad (2)$$

Where, C_0 is the adsorption-desorption equilibrium concentration of RhB and C is the concentration of RhB at reaction time of t.

3. Results and discussion

3.1 The development of g-C_3N_4 through self-condensation of guanidinium cyanurate

Figure 1a shows powder X-ray diffraction (XRD) pattrerns of g-C_3N_4 from melamine (CNM) and guanidinium cyanurate (CNG). There are two typical peaks: one at 13.10° and another at 27.48°. The former is ascribed to tri-*s*-triazine units (100). The later belongs to interlayer-stacking structures (002). The intensity of CNG's (002) peak is markedly lower than that of CNM. This indicates that g-C_3N_4 nanosheets are stacked in a very loose pattern. Graphitic- C_3N_4 nanosheets from liquid exfoliation [13b, 13d] show the same character. The as-synthesized CNG has the same FT-IR spectrum as CNM (Fig. 1b). The bands of 1200−1650 cm^{-1} are ascribed to the typical stretching modes of C-N heterocycles. The band at 814 cm^{-1} is ascribed to the breathing mode of triazine units. The bands between 3200 and 3500 cm^{-1} are ascribed to the N–H stretching modes. It is clearly demonstrated that g-C_3N_4 can be obtained through self-condensation of guanidinium cyanurate and g- C_3N_4 nanosheets show a loose stacking model.

The development of g-C_3N_4 nanosheets under different treatment temperature was characterized by powder XRD. The sample treated at 400 ℃ shows two intense peaks at 10.58° and 27.78° that indicates the low polymerization degree (Fig. 1c). When the condensation temperature increased to 450 ℃, two characteristic diffraction peaks (100) and (002) at 13.25° and 27.15° are detected, which suggest the incipient formation of g-C_3N_4. With the increasing heating temperature, the (100) peak tends to being weaker. This is caused by the decrease in thickness of g-C_3N_4 nanosheets [13a, 13c]. The treatment temperature directly influences the interlayer-stacking structure. As shown in Fig. 1d, when treatment temperature increased from 500℃ to 550℃, the (002) peak shifts from 27.15° to 27.48°. This indicates that layer-stacking structures are developed above 550℃.

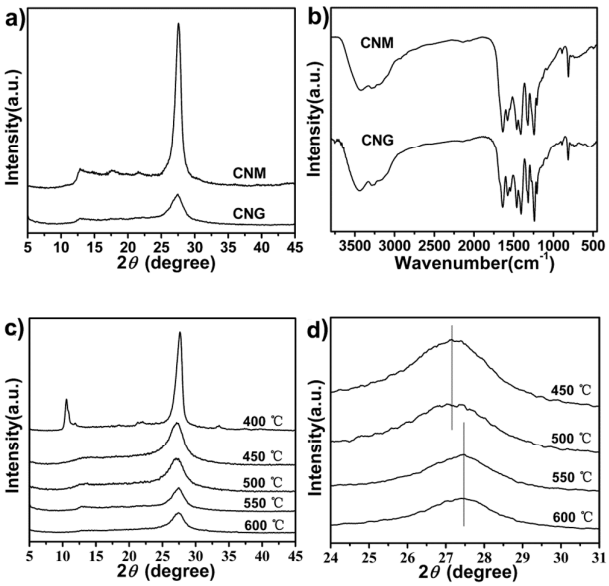

Fig. 1 a) Powder X-ray diffraction (XRD) pattrerns of g-C_3N_4 from melamine (CNM) and guanidinium cyanurate (CNG). b) FT-IR spectra of CNM and CNG. c) Powder XRD patterns of g-C_3N_4 nanosheets under different treatment temperature. d) Enlarged XRD peaks at 25°-30°.

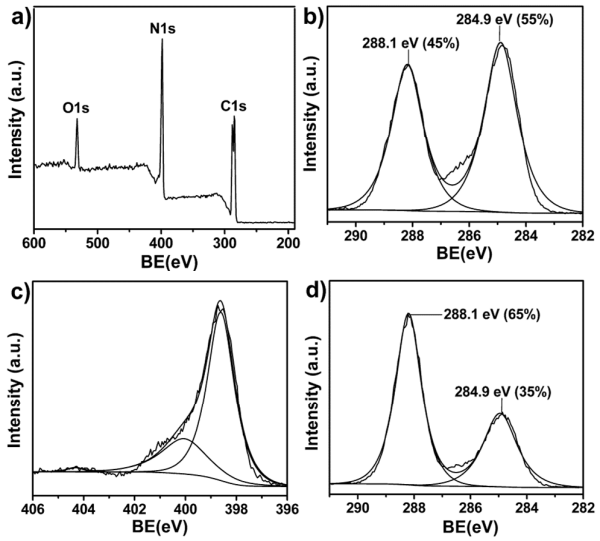

Fig. 2 a) XPS survey spectrum of CNG prepared at 550℃. b) C1s XPS peaks of CNG prepared at 550℃. c) N1s XPS peaks of CNG prepared at 550℃. d) C1s XPS peaks of CNG prepared at 450℃.

The chemical composition of CNG prepared at 550℃ was further characterized by XPS. XPS survey spectrum (Fig. 2a) shows that the main elements on the surface of are C, N. There is a small amount of oxygen, which is mainly attributed to the adsorbed water and carbon dioxide. The high-resolution XPS spectra of C1s can be fitted into two peaks. The peak centered at 288.1 eV is attributed to tri-*s*-triazine units in lattice, and the peak centered at 284.9 eV is attributed to the pure carbon stemmed from the combustion of nitrogen in air atmosphere. [11c, 13a] The content of pure carbon is increased with the increasing heating temperature because nitrogen tends to be burned easily at a high temperature. The content of pure carbon is 35% when the heating temperature is 450℃, and it increases to 55% when the heating temperature is 550℃ (Fig. 2b, d). Fitting of N1s envelope results in identification of two peaks: one at 398.6 eV and another at 400.1 eV. The former is indexed to tri-*s*-triazine units

in lattice and the latter is attributed to nitrogen atoms at edge of g-C_3N_4 nanosheets.

3.2 Porosity properties and heat-driven stacking of g-C_3N_4 nanosheets

Nitrogen adsorption-desorption measurements are preformed to investigate porosity properties of GC-derived g-C_3N_4 prepared at different temperature. Fig. 3a shows isotherm curves of the samples prepared at 450℃, 500℃, 550℃ and 600℃. With the increase of treatment temperature, there is a marked change in porosity of the as-synthesized materials. The samples prepared at 450℃ and 500℃ have poor porosity. But the solids treated under 550℃ and 600℃ show improved porosity. Hysteresis loops appear when $P/P_0 > 0.7$, which indicates the occurrence of open pore matrixes. As revealed by BET surface area calculated from the isotherm curves (Fig. 3b), the values are below 50 m^2/g for the samples at 450℃ and 500℃ and sharply increase to 133.8 m^2/g when temperature reaches 550℃. Very high BET surface area of 194.7 m^2/g is achieved under treatment temperature of 600℃. Pore volume also exhibits a markedly increasing curve with treatment temperature (Fig. 3c). However, average pore size (calculated based on BJH desorption model) shows an unexpected fluctuation with the increase of treatment temperature (Fig. 3d). The value sharply increases to 8.45 nm at 550℃ and then decreases to 1.53 nm at 600℃. There may be a microstructure transform mechanism for this heat-driven development of porosity.

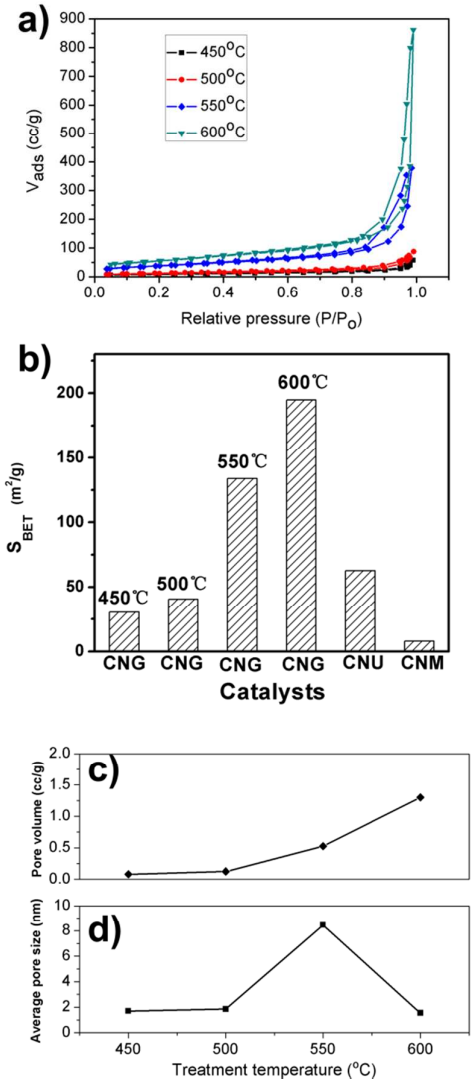

Fig. 3 a) Nitrogen adsorption-desorption isotherm curves of CNGs prepare at different temperature. b) BET surface area of CNG, CNU, and CNM. c) Pore volume of CNGs prepare at different temperature. d) Average pore size CNGs prepare at different temperature.

TEM measurements are performed to investigate this heat-driven microstructure transform mechanism. The materials prepared at 450℃ have microstructures of thick stacking layers (Fig. 4a). When treated at 500℃, sub-structures are developed in the stacking layers. Honeycombed layers are observed (Fig. 4b). When treatment

temperature is increased to 550℃, very thin g-C_3N_4 nanosheets are formed and their sizes reach 1.0 μm× 1.0 μm (Fig. 4c, d). Large g-C_3N_4 nanosheets are stacked in a state similar to randomly creased paper slips. These microstructures lead to high porosity of the bulk materials, which has been demonstrated by nitrogen adsorption-desorption measurements. BET surface area values of the samples at 450℃ and 500℃ are below 50 m^2/g, but when temperature reaches 550℃, it sharply increases to 133.8 m^2/g. As revealed by Fig. 3c, g-C_3N_4 nanosheets show large two-dimension size and pore systems formed by a randomly stacking and creasing model have relatively large average pore size. The calculated pore size is 8.45 nm, but the value is approximately 1.8 nm for the materials treated at 500℃ (Fig. 3d). Figure 4d shows that g-C_3N_4 nanosheets have one to three layers and their thickness is in the range from 0.6 nm to 1.5 nm. Further increase of treatment temperature to 600℃ results in curl and fragmentation of g-C_3N_4 nanosheets (Fig. 4 e, f). The curled and fragmented g-C_3N_4 nanosheets build up a highly porous matrix, which has BET surface area of 194.7 m^2/g. It is inevitable that curl and fragmentation of g-C_3N_4 nanosheets directly lead to decrease of average pore size. The value is 1.53 nm at 600℃. It is clearly revealed that heat-driven transform of g-C_3N_4 nanosheets' microstructures determines the development of porosity properties.

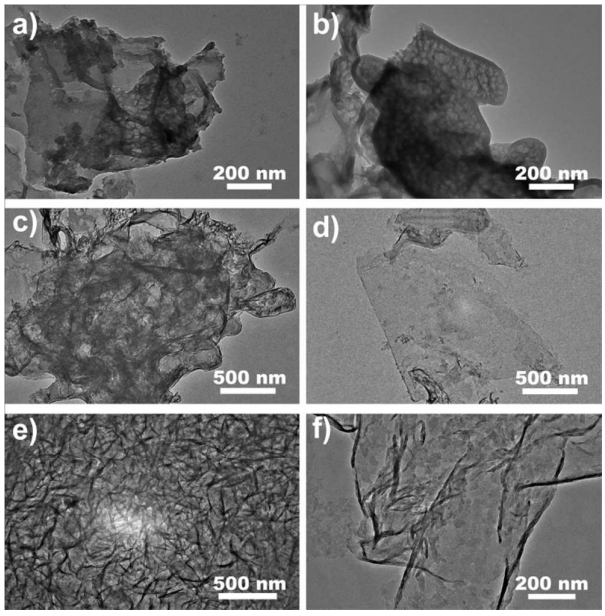

Fig. 4 TEM images of CNG at 450℃ (a), 500℃ (b), 550℃ (c, d), and 600℃ (e, f).

The morphological structures of the CNG prepared at different treatment temperatures are further characterized by scanning electron microscope (SEM). As shown in Fig. 5a, b, the materials prepared at 450℃ and 500℃ consist of thick layer-like structures that are packed in a random model. After being treated at 550℃, uniform g-C_3N_4 nanosheets are achieved and their thicknesses are sharply reduced (Fig. 5c). This is in accordance with the information revealed by TEM images (Fig. 4c, d). Further treatment at 600℃ lead to curl and fragmentation of g-C_3N_4 nanosheets (Fig. 5d). This trend is also demonstrated by TEM measurements (Fig. 4e, f). Treatment at high temperature in air directly leads to over-oxidation of g-C_3N_4 nanosheets and then fragments those microstructures. With the decrease thickness of g-C_3N_4 nanosheets under high temperature, the edges of nanosheets tend to curl and then reduce the large surface energy in nanometre scale.

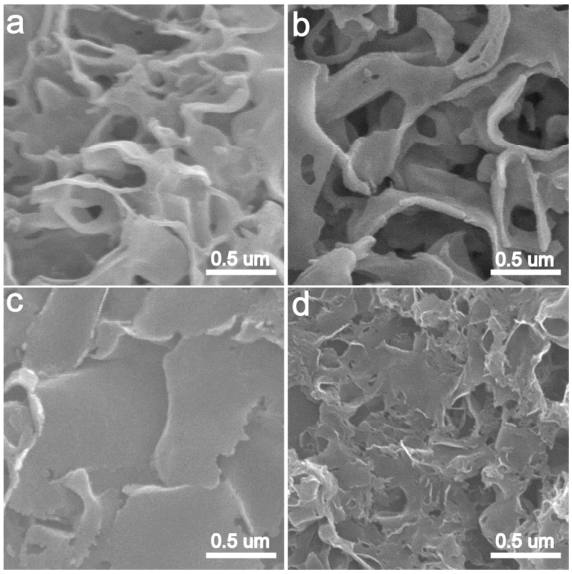

Fig. 5 SEM images of CNG at 450℃ (a), 500℃ (b), 550℃ (c), and 600℃ (d).

3.3 The optical properties of porous g-C_3N_4

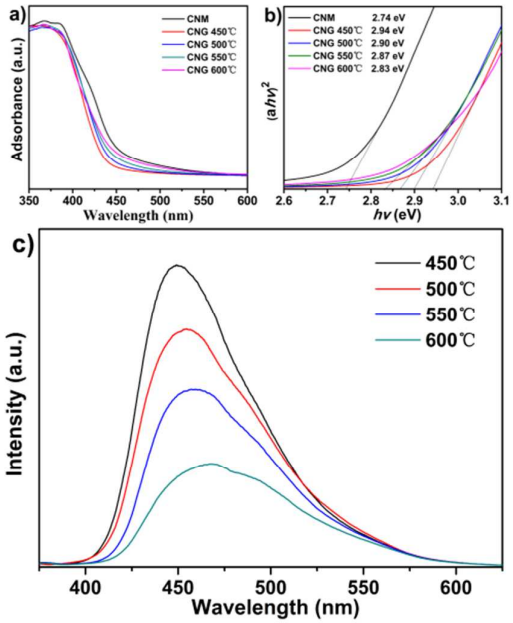

Fig. 6 a) UV-visible absorption spectra. b) Plots of $(ahv)^2$ versus energy (hv) of CNM and CNG. c) PL spectra of CNG obtained at different temperatures.

The UV-visible absorption spectra are used to investigate the optical absorption of g-C_3N_4 nanosheets. Fig. 6a shows that both CNM and CNG have strong UV and visible light absorption. The absorption edge of CNG shows an obvious blue shift from that of CNM. The band gap is 2.74 eV for CNM and the value increases to 2.87 eV for CNG (Fig .6b). This trend has been found in other g-C_3N_4 nanosheets and nanoparticles [13a, 13c, 13d, 18]. With the increase of heating temperature from 450 to 600℃, the absorption edge of CNG exhibits a continual blue shift. The optical absorption of the samples is further improved [19].

The photoluminescence (PL) spectra of CNG were also recorded. As presented in Fig. 6c, all samples exhibit a broad emission peak. The emission peak shows a slight blue shift from 449 nm to 470 nm when heating temperature increases from 450 ℃ to 600℃. PL intensity decreases gradually with the increase of heating temperature. This is attributed to the enhanced quantum confinement effect and the increased surface carbon

content [8b, 20]. The thickness of g-C_3N_4 nanosheets decreases sharply with the increase of treatment temperature. Fragmentation and stacking are gradually developed and attributed to the blue shift of PL spectra. The decrease of PL intensity implies that efficiency for the separation of charge carriers is improved [21], and beneficial for the photocatalytic performance.

3.4 The photocatalytic activity and stability of porous g-C_3N_4

The photocatalytic activity of porous g-C_3N_4 nanosheets is evaluated by the degradation of RhB under light irritation. The catalysts prepared from melamine (CNM) and urea (CNU) are tested under the same reaction conditions. Before reaction, the reaction mixtures are stirred in dark for 1 h to ensure that the adsorption equilibrium is established. The adsorption capacity of the g-C_3N_4 increases with their S_{BET} surface area and the amount is less than 15%. The degradation rate is calculated after the effect of adsorption has been eliminated. Direct degradation of RhB was negligible without the presence of any catalyst [22]. As shown in Fig. 7a, RhB can be degraded gradually under light irritation after CNM is added. The degradation rate is 22% after 60 min reaction. The catalytic activity of CNG and CNU are much higher than that of CNM. For CNU, 84% of RhB is degraded. CNG prepared at 550℃ can degrade 98% of RhB. The high photocatalytic activity of CNG is related to its large BET surface area. As shown in Fig. 3b, the S_{BET} of CNM and CNU are 8.0 $m^2 g^{-1}$ and 62.8 $m^2 g^{-1}$. The values are below 50 m^2/g for the samples at 450℃ and 500℃ and sharply increase to 133.8 m^2/g when temperature reaches 550℃. Very high BET surface area of 194.7 m^2/g is achieved under treatment temperature of 600℃. The catalysts with high porosity show improved photoactivity. High porosity provides more available catalytic active sites and benefits for diffusion of the reactants. Another important factor related to photocatalytic activity is improvement of optical properties with the development of g-C_3N_4 nanosheets with the increase of heating temperature. With the increase of heating temperature from 450 ℃ to 600℃, the optical absorption of the samples is further improved. PL intensity decreases gradually with the increase of heating temperature. The decrease of PL intensity implies that efficiency for the separation of charge carriers is improved, and beneficial for the photocatalytic performance.

Reaction rate constants of RhB degradation over different catalysts are calculated based on the first-order model (Fig. 7b). The degradation rate constant for CNM is 0.0041 min^{-1} and it increases to 0.031 for CNU. The largest rate constant of 0.055 min^{-1} is achieved when the reaction is catalyzed by CNG prepared at 600℃. The value is 13.41 and 1.78 times as high as those of CNM and CNU. The high stability is a special advantage of g-C_3N_4 as photocatalysts [4e, 23]. A five-run recycling test of RhB degradation is performed over CNG prepared at 550. The catalysts are separated by centrifugation and directly recycled into the next batch. The degradation rate of RhB has not decreased significantly during the five-run test. It dropped slightly from 98% in the first run to 91% in the fifth run. Graphitic-C_3N_4 nanosheets show excellent stability and recyclabiltiy for catalyzing RhB degradation.

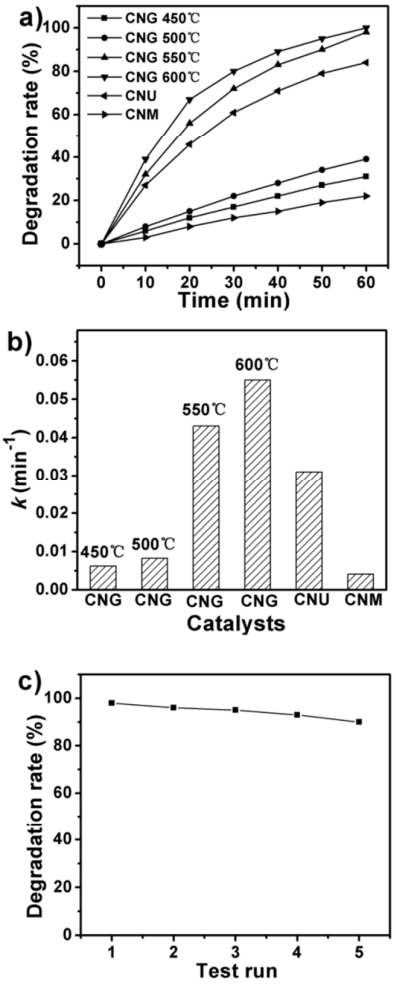

Fig. 7 a) Photocatalytic activity for RhB degradation. b) Reaction rate constants of RhB degradation over different catalysts. c) Recyclability of CNG obtained at 550℃ for RhB degradation.

4. Conclusions

In summary, nanoporous g-C_3N_4 materials have been successfully prepared through self-condensation of guanidinium cyanurate (GC) under heat treatment during 550-600 ℃ in air atmosphere without the assistance of any template. Porosity of these materials is developed through heat-driven stacking of g-C_3N_4 nanosheets. The mechanism is detailedly revealed through TEM and N_2 adsorption measurement. The BET surface area of as-synthesized materials at 600 ℃ nearly reaches 200 m^2/g. The photocatalytic activity of g-C_3N_4 nanosheets is evaluated by rhodamine (RhB) degradation under light irritation, and compared with that of samples and prepared from melamine (CNM) and urea (CNU) under the same conditions. The samples with higher surface area exhibit better optical properties and have enhanced photocatalytic activity.

Acknowledgements

This work was supported by the Natural Science Foundation of China (21304101, 21101161, 21174148).

Notes and references

Beijing National Laboratory of Molecular Science, Laboratory of Green Printing, Institute of Chemistry, Chinese Academy of Sciences, Beijing (PR China). Fax: (+86) 10-62559373; E-mail: lifb@iccas.ac.cn, yuangq@iccas.ac.cn

1 A. Fujishima, K. Honda, *Nature*, 1972, 238, 37-38.
2 a)K. Maeda, *Chem. Commun.*, 2013, 49, 8404-8406; b)K. Ikeue, Y. Shinmura, M. Machida, *Appl. Catal. B*, 2012, 123-124, 84-88; c)Y. Cong, H. S. Park, H. X. Dang, F.-R. F. Fan, A. J. Bard, C. B. Mullins, *Chem. Mater.*, 2012, 24, 579-586; d)Y. Wang, Y. Wang, R. Jiang, R. Xu, *Ind. Eng. Chem. Res.*, 2012, 51, 9945-9951.
3 a) X. F. Chen, J. S. Zhang, X. Z. Fu, M. Antonietti, X. C. Wang, *J. Am. Chem. Soc.*, 2009, 131, 11658-11659; b) X. Song, J. Hu, H. Zeng, *J. Mater. Chem. C*, 2013, 1, 2952-2969; c) H. Zeng, C. Zhi, Z. Zhang, X. Wei, X. Wang, W. Guo, Y. Bando, D. Golberg, *Nano Lett*. 2010, 10, 5049–5055.
4 a)A. Thomas, A. Fischer, F. Goettmann, M. Antonietti, J.-O. Müller, R. Schlögl, J. M. Carlsson, *J. Mater. Chem.*, 2008, 18, 4893-4908; b)Y. Zheng, J. Liu, J. Liang, M. Jaroniec, S. Z. Qiao, *Energy Environ. Sci.*, 2012, 5, 6717-6731; c)X. Wang, S. Blechert, M. Antonietti, *ACS Catal.*, 2012, 2, 1596-1606; d)X. H. Li, M. Antonietti, *Chem. Soc. Rev.*, 2013, 42, 6593-6604; e)Y. Wang, X. Wang, M. Antonietti, *Angew. Chem., Int. Ed.*, 2012, 51, 68-89.
5 B. Jurgens, E. Irran, J. Senker, P. Kroll, H. Muller, W. Schnick, *J. Am. Chem. Soc.*, 2003, 125, 10288-10300.
6 a)G. Zhang, M. Zhang, X. Ye, X. Qiu, S. Lin, X. Wang, *Adv. Mater.*, 2014, 26, 805-809; b)Y. Wang, J. Zhang, X. Wang, M. Antonietti, H. Li, *Angew. Chem., Int. Ed.*, 2010, 49, 3356-3359; c)Y. Wang, Y. Di, M. Antonietti, H. Li, X. Chen, X. Wang, *Chem. Mater.*, 2010, 22, 5119-5121; d)X. Wang, X. Chen, A. Thomas, X. Fu, M. Antonietti, *Adv. Mater.*, 2009, 21, 1609-1612; e)G. Liu, P. Niu, C. H. Sun, S. C. Smith, Z. G. Chen, G. Q. Lu, H. M. Cheng, *J. Am. Chem. Soc.*, 2010, 132, 11642-11648.
7 a)M. Bledowski, L. Wang, A. Ramakrishnan, O. V. Khavryuchenko, V. D. Khavryuchenko, P. C. Ricci, J. Strunk, T. Cremer, C. Kolbeck, R. Beranek, *Phys. Chem. Chem. Phys*., 2011, 13, 21511-21519; b)X. Zhou, B. Jin, L. Li, F. Peng, H. Wang, H. Yu, Y. Fang, *J. Mater. Chem.*, 2012, 22, 17900-17905; c)H. Yan, H. Yang, *J. Alloys Compd*., 2011, 509, L26-L29; d)S. Chen, Y. Hu, S. Meng, X. Fu, *Appl. Catal. B*, 2014, 150-151, 564-573.
8 a)S. Yang, X. Feng, X. Wang, K. Mullen, *Angew. Chem., Int. Ed.*, 2011, 50, 5339-5343; b)Y. Sun, C. Li, Y. Xu, H. Bai, Z. Yao, G. Shi, *Chem. Commun.*, 2010, 46, 4740-4742; c)Q. Liu, J. Zhang, Langmuir, 2013, 29, 3821-3828; d)Q. Xiang, J. Yu, M. Jaroniec, *J. Phys. Chem. C*, 2011, 115, 7355-7363; e)X. Bai, L. Wang, Y. Wang, W. Yao, Y. Zhu, *Appl. Catal. B*, 2014, 152-153, 262-270; f)Y. Sui, J. Liu, Y. Zhang, X. Tian, W. Chen, *Nanoscale*, 2013, 5, 9150-9155.
9 a)C. Liu, L. Jing, L. He, Y. Luan, C. Li, *Chem. Commun.*, 2014, 50, 1999-2001; b)K. Maeda, X. C. Wang, Y. Nishihara, D. L. Lu, M. Antonietti, K. Domen, *J. Phys. Chem. C*, 2009, 113, 4940-4947.
10 a)G. Zhang, X. Wang, *J. Catal.*, 2013, 307, 246-253; b)J. Zhang, G. Zhang, X. Chen, S. Lin, L. Mohlmann, G. Dolega, G. Lipner, M. Antonietti, S. Blechert, X. Wang, *Angewandte Chemie* 2012, 51, 3183-3187; c)Y. Cui, Z. Ding, X. Fu, X. Wang, *Angew. Chem., Int. Ed.*, 2012, 51, 11814-11818; d)J. Zhang, X. Chen, K. Takanabe, K. Maeda, K. Domen, J. D. Epping, X. Fu, M. Antonietti, X. Wang, *Angew. Chem., Int. Ed.*, 2010, 49, 441-444.
11 a)F. Goettmann, A. Fischer, M. Antonietti, A. Thomas, *Angew. Chem., Int. Ed.*, 2006, 45, 4467-4471; b)Y. Wang, J. Yao, H. Li, D. Su, M. Antonietti, *J. Am. Chem. Soc.*, 2011, 133, 2362-2365; c)Z. Huang, F. Li, B. Chen, T. Lu, Y. Yuan, G. Yuan, *Appl. Catal. B*, 2013, 136-137, 269-277; d)L. Jia, H. Wang, D. Dhawale, C. Anand, M. A. Wahab, Q. Ji, K. Ariga, A. Vinu, *Chem. Commun.*, 2014, 50, 5976-5979.
12 a)A. H. Castro Neto, N. M. R. Peres, K. S. Novoselov, A. K. Geim, *Rev. Mod. Phys*., 2009, 81, 109-162; b)J. Baringhaus, M. Ruan, F. Edler, A. Tejeda, M. Sicot, A. Taleb-Ibrahimi, A. P. Li, Z. Jiang, E. H. Conrad, C. Berger, C. Tegenkamp, W. A. de Heer, *Nature* 2014, 506, 349-354; c)R. K. Joshi, P. Carbone, F. C. Wang, V. G. Kravets, Y. Su, I. V. Grigorieva, H. A. Wu, A. K. Geim, R. R. Nair, Science 2014, 343, 752-754; d)X. Zheng, J. Xu, K. Yan, H. Wang, Z. Wang, S. Yang, *Chem. Mater.*, 2014, 26, 2344-2353; e)Y. Jiao, Y. Zheng, M. Jaroniec, S. Z. Qiao, *J. Am. Chem. Soc.*, 2014, 136, 4394-4403; f)K. S. Novoselov, Z. Jiang, Y. Zhang, S. V. Morozov, H. L. Stormer, U. Zeitler, J. C. Maan, G. S. Boebinger, P. Kim, A. K. Geim, Science 2007, 315, 1379-1379; g)A. K. Geim, K. S. Novoselov, Nature Materials 2007, 6, 183-191.
13 a)P. Niu, L. Zhang, G. Liu, H.-M. Cheng, *Adv. Funct. Mater.*, 2012, 22, 4763-4770; b)J. Xu, L. Zhang, R. Shi, Y. Zhu, *J. Mater. Chem. A*, 2013, 1, 14766-14772; c)X. Zhang, X. Xie, H. Wang, J. Zhang, B. Pan, Y. Xie, *J. Am. Chem. Soc.*, 2013, 135, 18-21; d)S. Yang, Y. Gong, J. Zhang, L. Zhan, L. Ma, Z. Fang, R. Vajtai, X. Wang, P. M. Ajayan, *Adv. Mater.*, 2013, 25, 2452-2456; e)H. Zhao, H. Yu, X. Quan, S. Chen, Y. Zhang, H. Zhao, H. Wang, *Appl. Catal. B*, 2014, 152-153, 46-50; f)J. Tian, Q. Liu, A. M. Asiri, A. O. Al-Youbi, X. Sun, *Anal. Chem.*, 2013, 85, 5595-5599; g)X. L. Zhang, C. Zheng, S. S. Guo, J. Li, H. H. Yang, G. Chen, *Anal. Chem.*, 2014, 86, 3426-3434; h)J. Tian, Q. Liu, C. Ge, Z. Xing, A. M. Asiri, A. O. Al-Youbi, X. Sun, *Nanoscale*, 2013, 5, 8921-8924; i)J. Tian, Q. Liu, A. M. Asiri, A. H. Qusti, A. O. Al-Youbi, X. Sun, *Nanoscale*, 2013, 5, 11604-11609; j)S. Tonda, S. Kumar, S. Kandula, V. Shanker, *J. Mater. Chem. A*, 2014, 2, 6772-6780; k)L.-S. Lin, Z.-X. Cong, J. Li, K.-M. Ke, S.-S. Guo, H.-H. Yang, G.-N. Chen, *J. Mater. Chem. B*, 2014, 2, 1031-1037; l)Z. Z. Lin, X. C. Wang, *Angew. Chem., Int. Ed.*, 2013, 52, 1735-1738.
14 a)J. N. Coleman, M. Lotya, A. O'Neill, S. D. Bergin, P. J. King, U. Khan, K. Young, A. Gaucher, S. De, R. J. Smith, I. V. Shvets, S. K. Arora, G. Stanton, H. Y. Kim, K. Lee, G. T. Kim, G. S. Duesberg, T. Hallam, J. J. Boland, J. J. Wang, J. F. Donegan, J. C. Grunlan, G. Moriarty, A. Shmeliov, R. J. Nicholls, J. M. Perkins, E. M. Grieveson, K. Theuwissen, D. W. McComb, P. D. Nellist, V. Nicolosi, *Science* 2011, 331, 568-571; b)D. Hanlon, C. Backes, T. M. Higgins, M. Hughes, A. O'Neill, P. King, N. McEvoy, G. S. Duesberg, B. Mendoza Sanchez, H. Pettersson, V. Nicolosi, J. N. Coleman, *Chem. Mater.*, 2014, 26, 1751-1763; c)A. Anto Jeffery, C. Nethravathi, M. Rajamathi, *J. Phys. Chem. C*, 2014, 118, 1386-1396; d)G. Cunningham, M. Lotya, C. S. Cucinotta, S. Sanvito, S. D. Bergin, R. Menzel, M. S. P. Shaffer, J. N. Coleman, *Acs Nano*, 2012, 6, 3468-3480.
15 a)J. Liu, T. Zhang, Z. Wang, G. Dawson, W. Chen, *J. Mater. Chem.*, 2011, 21, 14398-14401; b)F. Dong, L. Wu, Y. Sun, M. Fu, Z. Wu, S. C. Lee, *J. Mater. Chem.*, 2011, 21, 15171-15174; c)Y.-P. Yuan, W.-T. Xu, L.-S. Yin, S.-W. Cao, Y.-S. Liao, Y.-Q. Tng, C. Xue, *Int. J. Hydrogen Energy*, 2013, 38, 13159-13163; d)Y. Zhang, J. Liu, G. Wu, W. Chen, *Nanoscale*, 2012, 4, 5300-5303; e)D. Gao, Q. Xu, J. Zhang, Z. Yang, M. Si, Z. Yan, D. Xue, *Nanoscale*, 2014, 6, 2577-2581.
16 a)M. Shalom, S. Inal, C. Fettkenhauer, D. Neher, M. Antonietti, *J. Am. Chem. Soc.*, 2013, 135, 7118-7121; b)Y. S. Jun, J. Park, S. U. Lee, A. Thomas, W. H. Hong, G. D. Stucky, *Angew. Chem., Int. Ed.*, 2013, 52, 11083-11087; c)Y.-S. Jun, E. Z.

Lee, X. Wang, W. H. Hong, G. D. Stucky, A. Thomas, *Adv. Funct. Mater.*, 2013, 23, 3661-3667; d)G. Zhang, J. Zhang, M. Zhang, X. Wang, *J. Mater. Chem.*, 2012, 22, 8083-8091; e)G. Dong, L. Zhang, *J. Mater. Chem.*, 2012, 22, 1160-1166; f)F. Dong, Y. Sun, L. Wu, M. Fu, Z. Wu, *Catal. Sci. Technol.*, 2012, 2, 1332-1335; g)M. Tahir, C. Cao, F. K. Butt, F. Idrees, N. Mahmood, Z. Ali, I. Aslam, M. Tanveer, M. Rizwan, T. Mahmood, *J. Mater. Chem. A*, 2013, 1, 13949-13955 ; h)Y. Cui, J. Huang, X. Fu, X. Wang, *Catal. Sci. Technol.*, 2012, 2, 1396-1402; i)J. Zhang, J. Sun, K. Maeda, K. Domen, P. Liu, M. Antonietti, X. Fu, X. Wang, *Energy Environ. Sci.*, 2011, 4, 675-678; j)J. Xu, H. T. Wu, X. Wang, B. Xue, Y. X. Li, Y. Cao, *Phys. Chem. Chem. Phys*., 2013, 15, 4510-4517.

17 N. E.A. El-Gamel, J. Wagler, E. Kroke, *J. Mol. Struct.*, 2008, 888, 204 – 213.

18 a)S. Liu, J. Tian, L. Wang, Y. Luo, J. Zhai, X. Sun, *J. Mater. Chem.*, 2011, 21, 11726-11729; b)S. Liu, J. Tian, L. Wang, Y. Luo, X. Sun, *RSC Adv.*, 2012, 2, 411-413.

19 a)A. Du, S. Sanvito, Z. Li, D. Wang, Y. Jiao, T. Liao, Q. Sun, Y. H. Ng, Z. Zhu, R. Amal, S. C. Smith, *J. Am. Chem. Soc.*, 2012, 134, 4393-4397; b)Y. Zhang, T. Mori, L. Niu, J. Ye, *Energy Environ. Sci.*, 2011, 4, 4517-4521; c)G. Liao, S. Chen, X. Quan, H. Yu, H. Zhao, *J. Mater. Chem.*, 2012, 22, 2721-2726.

20 a)X. H. Li, J. S. Chen, X. Wang, J. Sun, M. Antonietti, *J. Am. Chem. Soc.*, 2011, 133, 8074-8077; b)H. Yan, *Chem. Commun.*, 2012, 48, 3430-3432.

21 a)S. Martha, A. Nashim, K. M. Parida, *J. Mater. Chem. A*, 2013, 1, 7816-7824; b)S. Zhao, S. Chen, H. Yu, X. Quan, *Sep. Purif. Technol.*, 2012, 99, 50-54.

22 a)J. Fu, Y. Tian, B. Chang, F. Xi, X. Dong, *J. Mater. Chem.*, 2012, 22, 21159-21166; b)L. Sun, X. Zhao, C.-J. Jia, Y. Zhou, X. Cheng, P. Li, L. Liu, W. Fan, *J. Mater. Chem.*, 2012, 22, 23428-23438; c)S. Ye, L.-G. Qiu, Y.-P. Yuan, Y.-J. Zhu, J. Xia, J.-F. Zhu, *J. Mater. Chem. A*, 2013, 1, 3008-3015; d)J. Di, J. Xia, S. Yin, H. Xu, L. Xu, Y. Xu, M. He, H. Li, *J. Mater. Chem. A*, 2014, 2, 5340-5351; e)L. Ye, J. Liu, Z. Jiang, T. Peng, L. Zan, *Appl. Catal. B*, 2013, 142-143, 1-7; f)T. Li, L. Zhao, Y. He, J. Cai, M. Luo, J. Lin, *Appl. Catal. B*, 2013, 129, 255-263.

23 E. G. Gillan, *Chem. Mater.*, 2000, 12, 3906-3912.